Mat. Res. Soc. Symp. Proc. Vol. 665 © 2001 Materials Research Society

Electronic Properties of Polymer-Fullerene Solar Cells

V. Dyakonov, I. Riedel, C. Deibel, J. Parisi, C. J. Brabec[1], N. S. Sariciftci[1], J.C. Hummelen[2]
Faculty of Physics, University of Oldenburg, D-26111 Oldenburg, Germany
[1]Linz Institute for Organic Solar Cells (LIOS), Physical Chemistry, Johannes Kepler University Linz, Altenbergerstraße 69, A-4040 Linz, Austria
[2]Stratingh Institute and MSC, University of Groningen, Nijenborgh 4, 9747 AG Groningen, The Netherlands

ABSTRACT

We studied the electronic transport properties of conjugated polymer/fullerene based solar cells by means of temperature and illumination intensity dependent current-voltage characteristics, admittance spectroscopy and light-induced electron spin resonance. The short-circuit current density increases with temperature at all light illumination intensities applied, i.e., from 100 mW/cm^2 to 0.1 mW/cm^2 (white light), whereas a temperature independent behavior was expected. An increase of the open-circuit voltage from 850 mV to 940 mV was observed, when cooling down the device from room temperature to 100 K. The fill factor depends strongly on temperature with a positive temperature coefficient in the whole temperature range. In contrast, the light intensity dependence of the fill factor shows a maximum of 52% at intermediate illumination intensities (3 mW/cm^2) and decreases subsequently, when increasing the intensity up to 100 mW/cm^2. Further studies by admittance spectroscopy revealed two frequency dependent contributions to the device capacitance. One, as we believe, originates from trapping states located at the interface between composite and metal electrode with an activation energy of E_A=180 meV, and the other one is from very shallow bulk states with E_A=10 meV. The origin of the latter is possibly the thermally activated conductivity. The photo-generation of charge carriers and their fate in these blends have been studied by light-induced electron spin resonance. We can clearly distinguish between photo-generated electrons and holes in the composites due to different spectroscopic splitting factors (g-factors). Additional information on the environmental axial symmetry of the holes located on the polymer chains as well as on a lower, rhombic, symmetry of the electrons located on the methanofullerene molecules has been obtained. The origin of the signals and parameters of the g-tensor have been confirmed from studies on a hole doped polymer.

INTRODUCTION

In recent years, the development of thin film plastic solar cells, using polymer-fullerene [1,2] or polymer-polymer [3] bulk heterojunctions as an absorber (and transport layer at the same time), has made significant progress. Efficiencies between 1% and >2.5% for laboratory cells under AM1.5 illumination conditions have been reported [2,3,4]. The typical structure of these devices consists of a composite of two materials with donor and acceptor properties, respectively, sandwiched between two electrodes. One of the most advanced combinations to date is the conjugated polymer poly (2-methoxy-5-(3-,7-dimethyl-octyloxy)-1,4-phenylene vinylene (MDMO-PPV) and the soluble Buckminster fullerene derivative [6,6] phenyl-C_{61}-butyric acid methyl ester (PCBM; a methanofullerene). One advantage of this type of device is the easy processability. The active layer is solution processed, by using spin-coating or doctor

blade techniques. Significant breakthrough has been achieved by realizing that the morphology of the composites plays an important role for the device performance [2,5]. In the case of MDMO-PPV:PCBM solar cells, the improved morphology has been achieved by using chlorobenzene as solvent [2]. It is clear that a morphology optimization should be performed for any combination of these materials.

The principle of operation of the above devices is based on the photoinduced electron transfer in donor-acceptor composites [6]. The charge transfer occurs within the sub-picosecond range, and the separated state is metastable. This may be described as ultrafast formation of pairs of $(D^+ \ldots A^-)$ - type which have a high rate of dissociation and a low rate of recombination. The formation of interpenetrating networks between processable conjugated polymers and fullerene derivatives in contrast to a flat interface (e.g., bilayer device) is an effective method to increase the charge generating interface in photovoltaic devices. A high spectral quantum yield of photo-generated charge carriers is therefore expected.

There remain several fundamental questions about the photo-physics and the carrier transport in these promising devices to be answered. The photoinduced forward electron transfer occurs on the time scale of at least 50 fs [7] and still needs to be explained. A controversy concerns the driving force for charge separation under short-circuit conditions. An extremely thin absorber thickness provides that the photo-generation of electrons and holes across the device thickness is quite homogeneous, therefore, the charge carrier density gradient across the device does not seem to be responsible for the effect. The polymer-fullerene network formed is bi-continuous, i.e., the electrons and holes have their own transport paths: the holes along the polymer chains towards the high work function ITO electrode, the electrons, in turn, via percolated fullerene molecules to the low work function electrode. The work functions difference of the electrodes is about 0.5 eV - 0.6 eV (χ_{ITO} = 4.8 eV - 4.9 eV, χ_{Al} = 4.3 eV) and might be responsible for the symmetry breaking. The solar cells will be electrical field driven in this case. However, the open circuit voltage obtained in our cells (see below) is much higher, therefore, the work function difference argument alone does not solve this problem. On the other hand, the electrodes represent selective membranes for the respective charges, so the cell should work also in the absence of the "built-in" field, and the situation is similar to the behavior of the dye-sensitized cells. In the latter case, the situation under illumination is described by the gradient of the quasi-Fermi energy for electrons and holes in the absorber layer (or by the gradient of the electrochemical potential), whereas the conditions for electron/hole extractions are fulfilled.

The electronic processes limiting the device performance are not yet known in all details. Studies of current density-voltage (J-V) characteristics of the ITO/PEDOT:PSS/MDMO-PPV:PCBM/Al solar cells as a function of the temperature and the illumination intensity may provide information on the charge transport properties, injection mechanisms, influence of defects (both bulk and interface ones) on the device performance.

Electrical spectroscopy performed by techniques such as admittance spectroscopy can contribute to the understanding of the defects in the polymer solar cells. The presence of the gap states as well as the interface states may influence the electrical parameters of the cell due to charge carrier trapping, and may act as recombination centers. This technique involves measurements of the conductance and capacitance of the junction as a function of the device temperature and, if necessary, the external applied bias voltage. The latter is superimposed to the small ac-voltage of variable frequency applied to the device.

EXPERIMENTAL DETAILS

We studied the current density-voltage (J-V) and capacitance-frequency-temperature (C(ω,T)) behavior of the ITO/PEDOT:PSS/MDMO-PPV:PCBM/Al structures. For this, a 1:3 (weight) blend of poly [2-methoxy-5-(3´,7´-dimethyl-octyloxy-)1,4-phenylene-vinylene] (MDMO-PPV), as an electron donor, and [6,6]-phenyl C_{61}-butyric acid methyl ester (PCBM), as the electron accepting moiety, was prepared in chlorobenzene. To reduce the surface roughness of the ITO covered glass substrates and to improve the matching of the work functions at the interface, an additional layer of the doped conjugated polymer PEDOT:PSS (Bayer AG) with 80 nm thickness was deposited by a spin-coating technique. Subsequently, a 100 nm active layer of MDMO-PPV:PCBM was spin cast from solution. As a back electrode we used aluminum, which was thermally evaporated in a vacuum chamber. The device structure of the prepared devices is displayed in Figure 1a.

For device characterization, we used a variable temperature cryostat which allows measurements in the temperature range of 4 K - 400 K. The devices were illuminated through a sapphire window by an xenon arc lamp whose intensity is controlled by a set of neutral density filters. Inside the cryostat, the maximum intensity is calibrated to 100 mW/cm^2. With the filter array it was possible to vary the illumination intensity by three orders of magnitude. In addition, the infrared part of the spectrum was reduced by using a water filter, in order to better match the illumination to the AM1.5-spectrum. With this experimental setup, the current-voltage measurements under variation of illumination intensity and temperature were performed.

Admittance measurements in the frequency range 0.1 Hz –10 MHz have been performed with a Solartron impedance analyzer 1260A equipped with a Solartron dielectric interface 1296A in combination with a variable temperature helium cryostat (T=20 K - 320 K). The measurements were carried out at an oscillator level of 30 mV without dc voltage, in order to work close to equilibrium, which can be distorted at high injection of charge carriers. Electron spin resonance (ESR) measurements were performed with a Bruker X-Band (9.5 GHz) and W-Band (95 GHz) spectrometer in combination with a variable temperature cryostat. For light induced ESR studies, the samples were illuminated with the 488 nm (≈ 2.5 eV) line of an Ar^+ laser.

Current density-voltage analysis

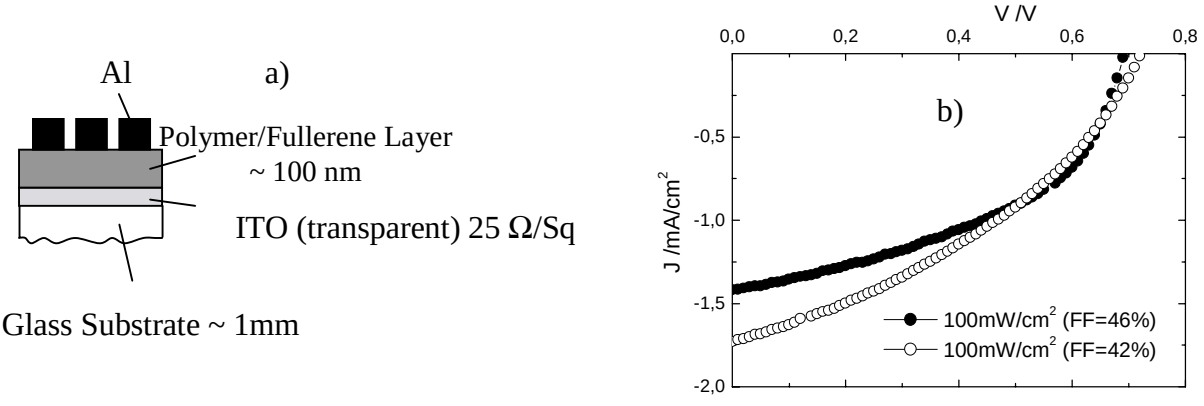

Figure 1. a) Configuration for of a ITO/MDMO-PPV:PCBM/Al device. (A layer of the doped conducting polymer PEDOT:PSS between ITO and the composite was added, but it is optional.); **b)** Current-voltage characteristics for two devices with different fill factors.

Figure 1b shows current density-voltage characteristics (fourth quadrant) for two devices illuminated with 100 mW/cm^2 (white light) at room temperature. The devices have a slightly different active layer thickness, resulting in different values of the short-circuit current density (1.4 mA/cm^2 and 1.75 mA/cm^2, respectively). The influence of the series resistance on the fill factor can thus be seen.

Incident light intensity dependence

The illumination intensity was varied by three orders of magnitude from 0.1 mW/cm^2 to 100 mW/cm^2. Figure 2a shows the short-circuit current density J_{SC} as a function of the incident light intensity at several temperatures. The short-circuit current density increases with the illumination intensity P_{LIGHT}. The behavior is close to linear at T=300 K, but deviates at lower temperatures. Figure 2b shows the dependence of the V_{OC} on the intensity of incident light. One can see that V_{OC} increases with intensity, and saturates at values of 800 mV. The values of V_{OC} of 600 mV are achieved already at intensities below 10 mW/cm^2.

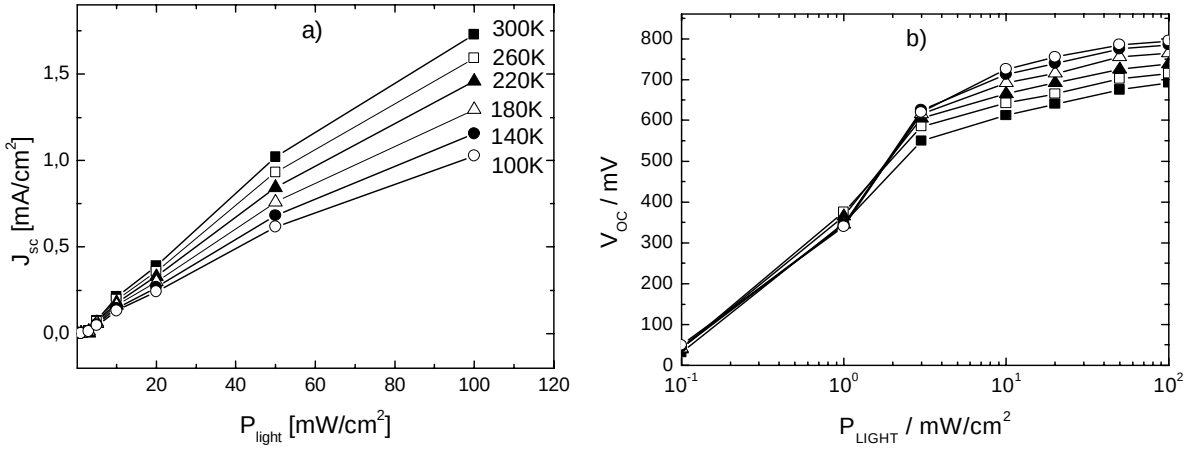

Figure 2. a) Short-circuit current density J_{SC} as a function of illumination intensity. The temperature varied from 100 K to 300 K;
b) open-circuit voltage versus illumination intensity. The symbols correspond to those in Fig. 2a.

While the short-circuit photo-current and the open-circuit voltage increase with illumination intensity, the fill factor, which is displayed in Figure 3, behaves in a different way. The fill factor is plotted versus P_{LIGHT} on a semi-logarithmic scale. The fill factor grows with P_{LIGHT} and reaches its maximum of 52% at T=300 K (full squares) at the light intensity of about 3 mW/cm^2. The further increase of the illumination intensity leads to a decrease of the fill factor for all temperatures.

Temperature dependence

The dependences of the device characteristics on temperature in the range from 100 K to 300 K were measured. Figure 4a shows the short-circuit current density as a function of temperature.

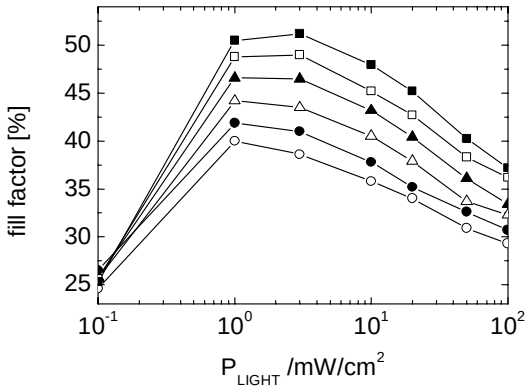

Figure 3. Fill factor as a function of illumination intensity. The temperature varied from 100 K (open circles) to 300 K (full squares) with steps of 40 K.

J_{SC} varies exponentially for all illumination intensities applied. This is surprising since a temperature independent J_{SC} behavior in inorganic solar cells is known and, therefore, expected.

The influence of temperature on the open-circuit voltage is displayed in Figure 4b. An increase of the open-circuit voltage from 850 mV to 940 mV is observed when cooling down the device from room temperature to 100 K. Qualitatively, this behavior was expected, and is typical for inorganic solar cells. For illumination intensities below 10 mW/cm^2, a slight decrease of V_{OC} with decreasing temperature is observed. This becomes more pronounced at temperatures between 100 K and 150 K. At the lowest illumination intensity, V_{OC} breaks down and a strong decrease in the whole temperature range is seen.

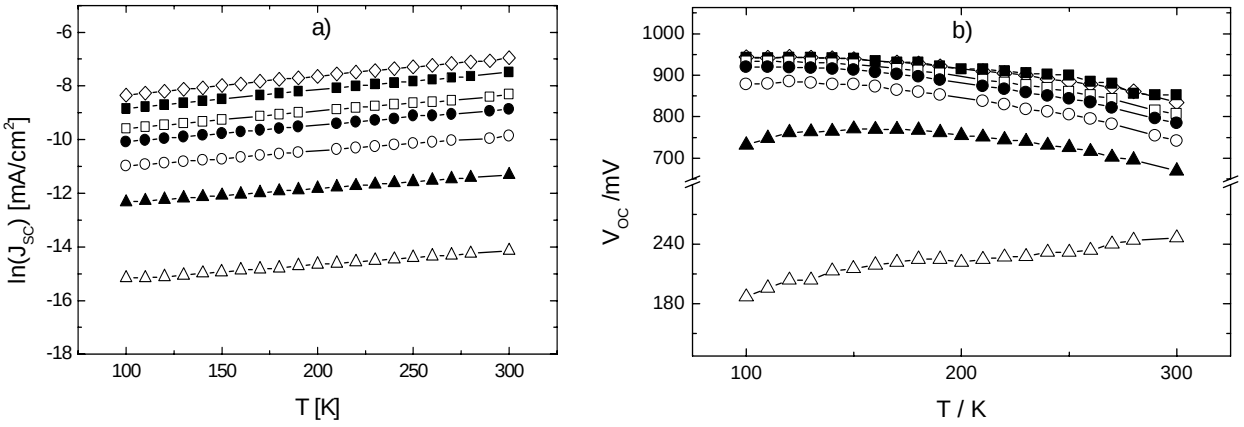

Figure 4. a) Temperature dependence of the short-circuit current density J_{SC}. The symbols correspond to different illumination intensities: 0.1 mW/cm^2 (open triangles), 1 mW/cm^2 (full triangles), 3 mW/cm^2 (open circles), 10 mW/cm^2 (full circles), 20 mW/cm^2 (open squares), 50 mW/cm^2 (full squares), 100 mW/cm^2 (open diamonds); **b)** open circuit voltage as a function of temperature.

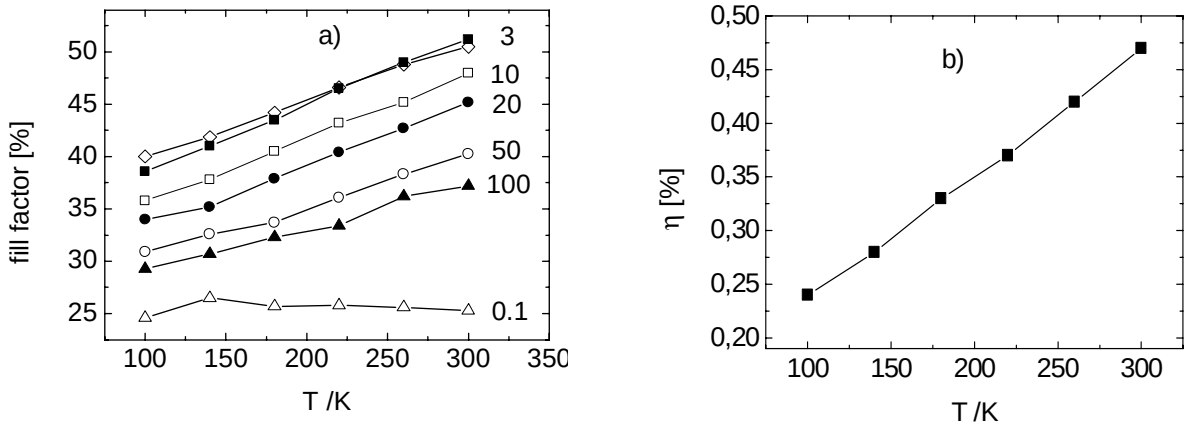

Figure 5. a) Fill factor vs. temperature for different intensities (in mW/cm^2); **b)** Power conversion efficiency vs. temperature. The device was illuminated with white light of 100 mW/cm^2.

The fill factor displayed in Figure 5a shows a positive temperature coefficient for all illumination intensities that are above 0.1 mW/cm^2. The effect can be due to a decrease of the series resistance. By combining the parameters V_{OC} and J_{SC} with the fill factor, the temperature behavior of the power conversion efficiency η of a solar cell can be estimated. This is shown in Figure 5b under white light illumination conditions with P_{LIGHT}=100 mW/cm^2. In the measured temperature range, a continuous increase of η with increasing temperature up to T=300 K is seen. The latter finding differs from that of inorganic devices, where the power conversion efficiency reaches its maximum between 200 K and 250 K and decreases afterwards.

Admittance spectroscopy

The frequency dependent contributions to the complex admittance, $Y=G+i\omega C$, can have several origins. They can originate from the thermally activated transport of free charge carriers, provided a space charge layer is present. Free charges respond at the frequency of the measurement until a certain critical frequency, at which the semiconductor behaves as a dielectric medium. Other contributions may originate from traps located in the bulk of the semiconductor material or at the interfaces due to the trapping and de-trapping of charge carriers in the energy levels. The presence of such states can be seen in the C(ω) dependence ($\omega=2\pi\nu$-angular frequency), where the characteristic steps are expected. The dependence of the capacitance C on the angular frequency ω is given by Eq. (1) [8]:

$$C \propto \frac{\omega_0^2}{\omega_0^2 + \omega^2}, \qquad (1)$$

where ω_0 is the emission rate of the defect $\omega_0 = 1/\tau = N_V v_{th} \sigma_p \exp(-E_A/kT)$. N_V is the effective density of states of the valence band, v_{th} the thermal velocity, and σ_p the capture cross section for holes. E_A is the activation energy of the trap. The above dependence is a step-like function with the parameter ω_0, which is temperature dependent and is given by Eq. (2):

$$\omega_0 = \xi_0 T^2 \exp\left(-\frac{E_A}{kT}\right), \qquad (2)$$

where T^2 is due to the fact that $v_{th} \propto T^{1/2}$ and $N_V \propto T^{3/2}$, ξ_0 is the temperature independent emission factor.

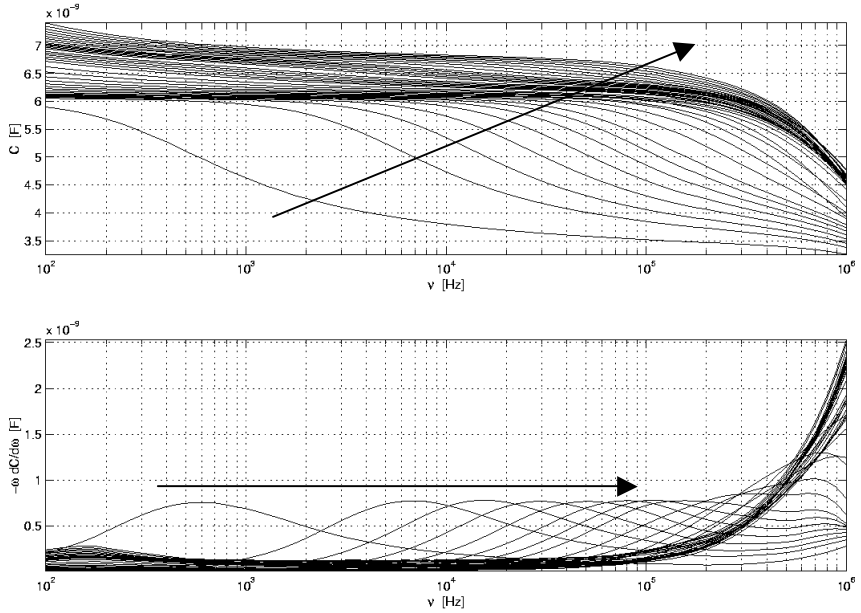

Figure 6. (top) Capacitance vs. frequency ($\nu=\omega/2\pi$) at different temperatures T=300 K-20 K (the spectra are not normalized with respect to the effective area of the device); (**bottom)** Differentiated capacitance vs. frequency. The arrow indicates the increase of the measurement temperature.

The dependence of the C(ω) response of an ITO/PEDOT:PSS/MDMO-PPV:PCBM/Al device at different temperatures is shown in Figure 6, top graph. (In the strict sense, the treatment of the imaginary part of the admittance as a capacitance is of limited validity and only true for a simple RC-circuit without resistance and inductance connected in series.) In the differentiated capacitance spectrum (see Fig.6, bottom graph), this step appears as a maximum, which reveals the position of the step on the frequency axis more accurately. The step shifts to lower frequencies, when cooling down the device from 300 K to 20 K. More informative, however, is the capacitance-temperature (see Fig.7, top graph) or the differentiated capacitance-temperature (see Fig. 7, bottom) analysis. One can clearly distinguish between two steps at different temperatures and, therefore, corresponding different activation energies. An Arrhenius evaluation of Figure 7 is shown in Figure 8. We calculated the activation energy and the pre-exponential emission factor to E_A=177 meV and $\xi_0=2.3\times10^3\ s^{-1}K^{-2}$ for one defect state and E_A=9 meV and $\xi_0=1.7\times10^3\ s^{-1}K^{-2}$ for the other, respectively.

Light-induced electron spin resonance

Electron spin resonance (ESR) is a proven technique for the investigation of the formation of unpaired spins (or radicals) in solid state. Light-induced ESR (LESR) is well suited for studies of the radical formation under the influence of light. LESR measurements on composites of conjugated polymers and fullerenes were already performed in a conventional X-band (9.5 GHz) spectrometer [10]. The results can be summarized as follows: No "dark" ESR signals have been found in films of pure MDMO-PPV and in PCBM. Instead, a strong light-induced ESR signal in the composite of these two substances was observed. The main finding was the formation of two

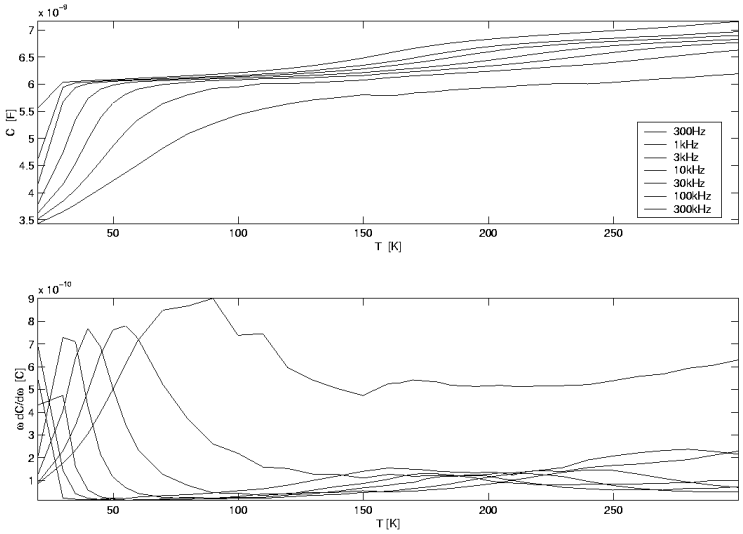

Figure 7. Capacitance (upper graph) and differentiated capacitance (lower graph) vs. temperature at different frequencies (indicated).

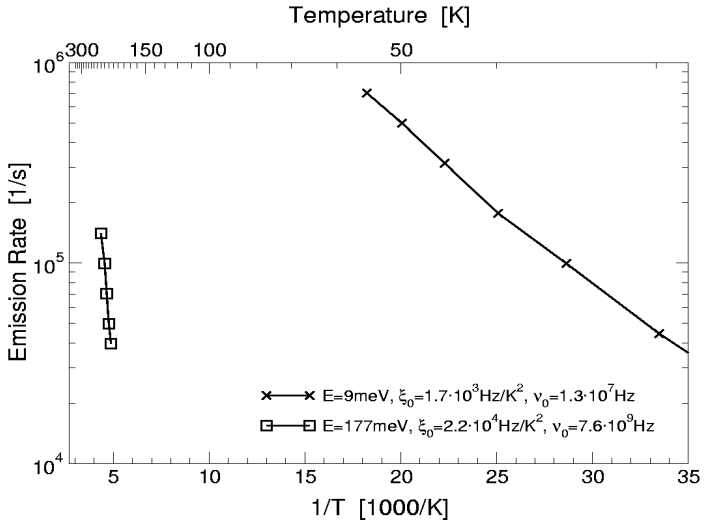

Figure 8. Arrhenius representation. The data are derived from Figure 7. The activation energy and the pre-exponential factors are defined in the text.

independent paramagnetic species (both with spin s=1/2) with slightly different g-factors ($g=h\nu/\mu_B B_0$): g_1=2.0025 and g_2=1.9995. The deviation of the g-factors of radicals in the conjugated π-electron systems from the free-electron value of 2.0023 is due to a non-compensated orbital moment, which induces an additional magnetic field. The latter is due to the transfer of the unpaired electron from the $\sigma_{C\text{-}C}$ orbital to the first excited state, i.e., the π^*-orbital, as discussed by Möbius [11]. Being a material constant, the g-factor allowed us to identify the signals as a positive polaron on the polymer chain (with g_1) and an electron accepted by the methanofullerene (with g_2). The small g-factor difference for both photo-generated species does not allow to study them separately due to a strong overlap of the ESR signals. (The overlap indeed contains some uncertainty in the interpretation of the signal as a superposition of two signals.) We found that the signals demonstrate a different saturation behavior, which is due to

different spin lattice relaxation times for the photo-generated species. This is an evidence of completely independent photo-induced spins without detectable spin-exchange-type correlation effects.

There is another way to separate the overlapping signals, i.e., to work at higher magnetic fields. This follows from the resonance condition $h\nu = g\,\mu_B\,B_0$ and implies, at the same time, the use of a higher microwave frequency. We carried out the experiments at approximately ten times higher magnetic fields and a ten times higher microwave frequency, i.e., 95 GHz instead of 9.5 GHz. Figure 9a shows the LESR spectrum measured at a microwave frequency of 95 GHz.

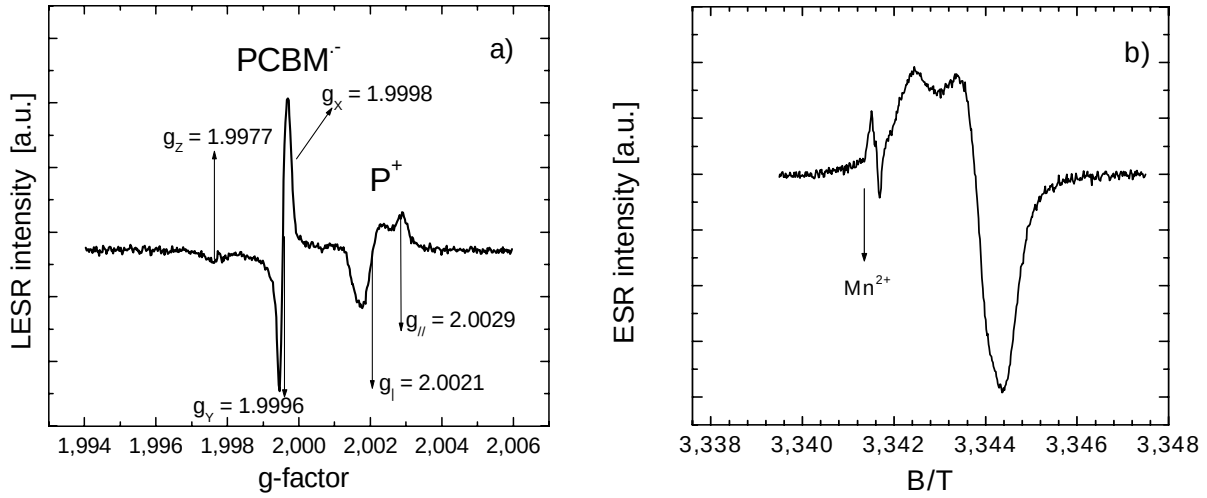

Figure 9. a) LESR spectrum of the MDMO-PPV/PCBM composite, showing the methanofullerene anion radical $PCBM^{\cdot -}$ and the positive polaron P^+. T=100 K, $\lambda_{exc.}$=488 nm.; **b)** ESR ("dark") spectrum of I_2-doped MDMO-PPV. T=100 K.

Two groups of lines, one from positive polarons on the polymer chain (P^+) and the second group from an electron on the methanofullerene molecule ($PCBM^{\cdot -}$ **)**, can clearly be seen. A highly improved resolution of the 95 GHz LESR not only allows to separate the signals and precisely determine their splitting factors (g-factors), but also to reveal a previously hidden structure within each group of lines. From the analysis of the line shape, we obtained information about the symmetry of the photo-generated species. The positive polaron on the polymer chain has an axial symmetry with the values of the g-tensor $g_\perp$=2.0029 and $g_\parallel$=2.0021. The PCBM radical anion has a lower, rhombic, symmetry with the values g_X = 1.9998, g_Y = 1.9996, g_Z = 1.9977.

DISCUSSION

We discuss now the temperature and incident light intensity dependences of the short-circuit current density, open-circuit voltage and fill factor of the ITO/PEDOT:PSS/MDMO-PPV-PCBM/Al solar cell. Let us first address the open-circuit voltage. We observed an increase of V_{OC} from 850 mV to 940 mV, when cooling the device down to 100 K. This behavior is typical for conventional inorganic pn-solar cells. The temperature dependence of V_{OC} is given by Eq. (3):

$$V_{OC} = \frac{k_B T}{q} \ln\left(\frac{J_{ph}}{J_0} + 1 \right), \quad (3)$$

where k_B is Boltzmann's constant, q the elementary charge, T the temperature, J_0 the saturation-current density, and J_{ph} the photo-current density. The dominant contribution is given by J_0, which is proportional to the product of the temperature and the intrinsic charge carrier density squared:

$$J_0 \propto n_i^2 T \propto T^4 \exp\left(-\frac{E_G}{kT} \right). \quad (4)$$

According to the Eq. (4), the exponential function determines the overall behavior, such that V_{OC} will increase at lower temperatures and, in the limit $T \rightarrow 0$ K, will reach the value E_G/q. In our heterojunctions, E_G is not the energy gap of the donor and acceptor materials in the blend, but rather the energy gap between the LUMO of the acceptor (the fullerene derivative) and the HOMO of the donor (conjugated polymer), which is approximately 1.1 eV. By extrapolating V_{OC} against $T \rightarrow 0$ K, the given value is quite reasonable. At lower temperatures (between 150 K and 100 K), a kink in $V_{OC}(T)$ can be seen (Fig. 4b). This becomes more and more pronounced at lower illumination intensities. It indicates the presence of the other factors, which determine V_{OC}. At the lowest intensity of 0.1 mW/cm^2, the open circuit voltage continuously decreases with temperature, which is due to the influence of a parallel resistance (R_P), which decreases with temperature.

The behavior of the short-circuit current density is even more unusual. One would expect a nearly temperature independent $J_{SC}(T)$ behavior, as it is the case in conventional inorganic solar cells. We, however, observe an exponential behavior for all intensities of incident light (see Fig. 4a). The series resistance (R_S), which depends strongly on temperature, might be responsible for the latter. One should also take into account the transport of the photo-generated electrons and holes within the fullerene and conjugated polymer transport paths, respectively.

A decrease of R_S at elevated temperatures (as well as an increase of R_P) influences the fill factor positively, as it is shown in Fig. 5a. (Being strongly temperature dependent, R_S seems to be less influenced by the light intensity.) The increase of J_{SC} and the fill factor results in a positive temperature coefficient of the power conversion efficiency $\eta = FF \times J_{SC} \times V_{OC} / W_{LIGHT}$, where W_{LIGHT} is the power density of the incident light (see Fig. 5b). This is quite a unique feature of the polymer-fullerene solar cells.

The fill factor was found to decrease at higher illumination intensity (>3 mW/cm^2) (see Fig. 3). The reason for this effect is unclear. This might be either due to a smaller parallel resistance, assuming that R_P is illumination intensity dependent, or due to an enhanced recombination of charge carriers. When the density of defects (in the bulk or at the interface) is high, the recombination current may become dominant. The presence of such defects was established by the admittance studies (see Fig. 8). Two frequency dependent contributions to the device capacitance were revealed, one of which, as we believe, originates from trapping states located at the interface between the composite and the metal electrode with an activation energy of E_A=180 meV, and the other one is a very shallow bulk state with E_A=10 meV. The origin of the latter is

possibly the thermally activated transversal conductivity. Decisive for the assignment of the capacitance peaks is the dependence of the activation energy on the external bias. These measurements are in progress. Our earlier studies [12] allowed us to conclude that the electrically active defect states, which we observe in the C(ω) dependences, are situated at the metal/polymer-composite interface. The bias independent position of the step is an evidence for Fermi level pinning at the interface due to the high density of defect states. We ruled out bulk defects, since the process of bulk defect ionization in conjugated polymers consists in the hopping of a hole from the conjugated segment with an acceptor impurity (compensated state) to the neighboring conjugated segment. Such hopping should be bias dependent due to the effective lowering of the potential barriers in high electric fields (Poole-Frenkel effect mechanism).

The photo-generation of charge carriers and their fate in these systems have been studied by light-induced electron spin resonance. We can clearly distinguish between photo-generated electrons and holes in the composites due to different spectroscopic splitting factors (g-factors). The application of high-frequency LESR to the conjugated polymer-(methano)fullerene blends led to a better understanding of the physics on the molecular scale. With this technique, one can better distinguish between photo-generated contributions to the LESR spectrum which are only slightly separated in the g-value. We were able to resolve a small g-anisotropy of each of the features. From the analysis of the line shape (see Fig. 9a), we obtained the information about the symmetry of the photo-generated species. The positive polaron on the polymer chain has an axial symmetry with the values of the g-tensor $g_{\perp} = 2.0029$ and $g_{\parallel} = 2.0021$. The PCBM radical anion has a lower, rhombic, symmetry with the values $g_X = 1.9998$, $g_Y = 1.9996$, $g_Z = 1.9977$.

To prove the idea of an axial symmetry of positive polarons P^+ on the polymer chain, another experiment was performed on MDMO-PPV. One can create positive polarons on the polymer by doping it with an acceptor. In this particular case, molecular iodine I_2 was used. At low degree of doping (the sample was exposed approximately 10 seconds to iodine vapor), the axial symmetry is again clearly visible (Fig. 9b). (Note, in this experiment the ESR was measured without illumination, since the charge transfer occurs in the ground state.) Also the g-tensor agrees, within the experimental error, with the one found for the P^+ spectrum in the blend. It can also be mentioned that, at longer exposure to the dopant, the ESR signal becomes significantly (ca. 25%) broader, from 1.05 mT to 1.33 mT for 5 min and 4 h of sublimation exposure, respectively, which results from an increase of the polaron concentration on the polymer chain due to dipole-dipole interaction. We did not observe any reduction in the intensity of the P^+ signal, which might be expected due to the bipolaron formation.

CONCLUSIONS

We have examined the electrical transport properties of novel polymer-fullerene solar cells by means of current-voltage characteristics and admittance spectroscopy in the temperature range 20-320 K. The current density increases with temperature at all light illumination intensities (from 100 mW/cm^2 to 0.1 mW/cm^2 white light) applied, whereas a temperature independent behavior was expected. An increase of the open-circuit voltage from 850 mV to 940 mV was observed when cooling down the device from room temperature to 100 K. The fill factor depends strongly on temperature, with a positive temperature coefficient in the whole temperature range. We conclude that the role of the series resistance (temperature dependence of the conductivity) is decisive for the device performance. By means of admittance spectroscopy, we were able to detect electrically active shallow levels with E_A=10 meV and E_A=180 meV.

An efficient generation of charge carriers and their fate in these systems have been studied by high frequency electron spin resonance. We can clearly follow the formation of photo-generated radical anion/radical cation pairs under illumination of the device absorber. Using high-frequency LESR, it was possible to separate these two contributions to the spectrum on the basis of their g-parameters, and to resolve the g-anisotropy of the radicals.

ACKNOWLEDGEMENTS

The authors would like to thank D. Godovsky, A. Gashti (University of Oldenburg), J. De Ceuster, E. Goovaerts (University of Antwerp), D. Meissner (University of Linz) for experimental support and for fruitful discussions. Research supported by German Research Council (DFG) under contract PA378/3-1.

REFERENCES

1. G. Yu, J. Gao, J. C. Hummelen, F. Wudl, and A. J. Heeger, *Science* **270,** 1789 (1995).
2. S. E. Shaheen, C. J. Brabec, F. Padinger, T. Fromherz, J. C. Hummelen, and N. S. Sariciftci, *Appl. Phys. Lett.* **78,** 841 (2001)
3. M Granström, K. Petritsch, A. C. Arias, A. Lux, M. R. Andersson, and R. H. Friend, *Nature* **395**, 257 (1998).
4. C. J. Brabec, S. E. Shaheen, M. T. Rispens, J. C. Hummelen, R. A. J. Janssen, D. Meissner, and N. S. Sariciftci, *Proceedings of the QUANTSOL 2001*, p. 28, Kirchberg, Austria.
5. J. J. M. Halls, A. C. Arias, J. D. MacKenzie, W. Wu, M. Inbasekaran, E. P. Woo, and R. H. Friend, *Adv. Mater.* **12**, 498 (2000).
6. N. S. Sariciftci, L. Smilowitz, A. J. Heeger, and F. Wudl, *Science* **258,** 1474 (1992).
7. C. J. Brabec, G. Zerza, G. Cerullo, S. De Silvestri, S. Luzzati, J. C. Hummelen, and N. S. Sariciftci (unpublished).
8. E. H. Nicollian and A. Goetzberger, *Appl. Phys. Lett.* **7**, 216 (1965).
9. R. Herberholz, M. Igalson, and H. W. Schock, *J. Appl. Phys.* **83**, 318 (1998).
10. V. Dyakonov, G. Zoriniants, M. Scharber, C. J. Brabec, R. A. J. Janssen, J. C. Hummelen, and N. S. Sariciftci, *Phys. Rev*. B **59,** 8019 (1999).
11. K. Möbius, *Z. Naturforsch.* **20a,** 1093 (1965).
12. V. Dyakonov, D. Godovsky, J. Parisi, C. J. Brabec, N. S. Sariciftci, J. C. Hummelen, J. De Ceuster, E. Goovaerts, Synth. Met. **1**, 8937 (2001).